JSTEM

Article

CNT-Al_2O_3-Ag-TiO_2 Nanocomposite for Stable Field Emission and Sensitive Low-pressure Hydrogen Detection

Yongxian Wu, Weijin Qian*, Zhuangzhuang Tian, Yifan Ji, Weijun Huang and Changkun Dong*

Wenzhou Key Lab of Micro-Nano Optoelectronic Devices, Wenzhou University, Wenzhou 325035, China; 18759325515@163.com (Y.W.); 18064764221@163.com (Z.T.); 13757504536@163.com (Y.J.); 18857757816@163.com (W.H.);
*Correspondence: weijinqian@wzu.edu.cn (W.Q.), dck@wzu.edu.cn (C.D.); Tel.: +86-577-86689067 (C.D.)

Abstract: Here we report the fabrication of a CNT-Al_2O_3-Ag-TiO_2 composite nanomaterial through a two-step process: (1) constructing the CNT-Al_2O_3-Ag composite on a silicon substrate using electrophoretic deposition (EPD), and (2) integrating Ti particles by magnetron sputtering followed by annealing. Comparing with the CNT-Al_2O_3 and CNT-Al_2O_3-Ag samples, the CNT-Al_2O_3-Ag-TiO_2 composite demonstrated the best field emission (FE) performance with a turn-on field of 2.1 V/μm and a threshold field of 4.76 V/μm. Under an oxygen pressure of 2×10^{-6} Pa, the CNT-Al_2O_3-Ag-TiO_2 composite exhibited the best stability with current fluctuations of about 2% at a current density of 2.5 mA/cm². In hydrogen sensing tests, the CNT-Al_2O_3-Ag-TiO_2 sample showed the best performance, displaying a 176% increase in sensing current at 5×10^{-4} Pa and an 87% increase at 8×10^{-6} Pa within 5 minutes at the initial current of 1.0 μA, highlighting its enhanced sensitivity. These results demonstrated that the CNT-Al_2O_3-Ag-TiO_2 nanocomposite is a promising candidate for field emission and high sensitive low-pressure hydrogen sensing applications.

Keywords: Carbon nanotubes (CNTs); Nanocomposite; Oxygen environment, Field emission; Low pressure; Hydrogen sensing

Received: April 26, 2025
Revised: May 6, 2025
Accepted: May 7, 2025
Published: May 11, 2025

Citation: Wu Y., Qian W., Tian Z., Ji Y., Huang W and Dong C. CNT-Al2O3-Ag-TiO2 Nanocomposite for Stable Field Emission and Sensitive Low-pressure Hydrogen Detection. Journal of STEM 2025, 2(1), 00004. https://doi.org/10.63460/MIAJ8898

1. Introduction

Carbon nanotubes (CNTs) have garnered substantial research interest in recent decades owing to their extraordinary electrical, thermal, and mechanical properties, making them the promising materials for various electronic applications, including field emission (FE) and gas sensing applications [1,2]. Advantages of low operation power, less thermal radiation, and quick start make the field emission sources attractive for various applications, such as X-ray sources and analytical instruments [3]. Nevertheless, the applications of CNT-based materials in harsh vacuum environments containing oxygen or other reactive gas agents could bring out significant technical challenges. The oxygen exposure could induce the oxidation and structural corrosion of CNTs, leading to the degradation of field emission currents [4,5]. On the other aspect, CNT-based gas sensors demonstrated remarkable potentials for hydrogen detections under atmospheric pressures, attributed to their exceptional sensitivity and fast response characteristics [6,7]. With the rapid development of vacuum microelectronics (VM) technology, the VM devices, such as X-ray tubes, microwave tubes, particle accelerators, mass spectrometers, and electron microscopes, need to be operated in high vacuum environments [8]. When the internal pressure of the vacuum device is less than 1×10^{-3} Pa, hydrogen gas is one of the main components of the residual gases in the vacuum device cavity. In addition, the small hydrogen molecular is easy to dissolve inside the device wall, and then release into the interior of the

vacuum system, which can also cause the pressure changes for the vacuum microelectronic devices in long term, significantly impacting the operation performances and service life [9]. Therefore, it is necessary to detect hydrogen contents in the VM devices. However, there are still limitations on reliable miniature low pressure hydrogen detection methods.

To address these limitations, researchers have explored various strategies, such as coating CNTs with protective layers or incorporating functional nanoparticles [10-15]. Among these approaches, the introduction of metal nanoparticles (e.g., Ag) and metal oxides has shown potentials on enhancing the emission stabilities for CNT-based composites [11,14]. Silver (Ag) nanoparticles are known for their excellent electrical conductivity and catalytic activity, benefiting the improvements of field emission and gas sensing properties [14,16]. Aluminum oxide (Al_2O_3) is particularly effective on enhancing the interfacial adhesion between CNTs and substrates due to strong electrostatic interactions and mechanical interlocking [17], thereby reducing the interfacial resistance, while its inherent secondary electron emission properties, to further enhance the field emission performance of CNT-based nanomaterials [18]. On the other hand, TiO_2 was introduced primarily due to its lower work function (~4.0 eV) compared to the CNTs [19], which could effectively decrease the overall work function of the CNT-based composite material. Meanwhile, titanium dioxide (TiO_2) offers high chemical stability and resistance to oxidation, making it an ideal protective layer for CNTs in complicated environments [20,21]. These effects optimize synergistically the field emission properties of the CNT-based nanocomposites. Besides, TiO_2 exhibited promising hydrogen sensing properties at atmospheric pressure [22], suggesting hydrogen detection potential under low-pressure conditions. By integrating Al_2O_3 and TiO_2, the CNT-based nanocomposite could enhance both the field emission and low pressure hydrogen sensing performance.

In this study, we synthesized CNT-Al_2O_3, CNT-Al_2O_3-Ag, and CNT-Al_2O_3-Ag-TiO_2 nanocomposites using a two-step method and their field emission and low pressure hydrogen sensing performance were evaluated. The incorporations of Al_2O_3, Ag and TiO_2 were designed to enhance the electrical and thermal properties and environmental stability of the CNT emitters. We systematically investigated the field emission properties, including turn-on field (E_{to}), threshold field (E_{thr}) and emission stability, as well as the hydrogen sensing performance of the materials. Our results demonstrated that the CNT-Al_2O_3-Ag-TiO_2 composite exhibits good field emission stability in oxygen environment and hydrogen sensing sensitivity, making it a promising candidate for electronic applications.

2. Materials and methods

2.1. Preparation of CNT-Based Nanocomposite Cathodes on Silicon Substrates

The CNT-based electrodes were synthesized on silicon substrates using EPD method [16,23]. To prepare CNT-based electrodes, the pristine CNTs (0.10 g/L, Shenzhen, China, Shenzhen Suiheng Graphene Technology Co., Ltd.) was first subjected to carboxylation treatment by immersing into the concentrated nitric acid under sonication. Subsequently, the treated CNTs were dispersed in an ethanol solution and sonicated for 2 hours to ensure a homogeneous suspension. Finally, the CNT electrode were fabricated via EPD, where the CNTs were deposited onto the silicon substrates under an applied electric field.

For the EPD synthesis of CNT-Al_2O_3 cathode, $Al(NO_3)_3$ and pristine CNTs (0.05g/L, 99.5%, Aladdin) was added to an ethanol solution. To synthesize CNT-Al_2O_3-Ag cathode, Ag powder (0.01 g/L, 99.5%, Aladdin) was mixed with the treated CNTs and $Al(NO_3)_3$ in ethanol. During the EPD process, the distance between the anode and cathode was set to 1 cm, with an applied voltage of 250 V and a deposition time of 2 minutes. For the preparation of CNT-Al_2O_3-Ag-TiO_2 cathode, a Ti layer was deposited on the surface of CNT-

Al_2O_3-Ag sample using radio frequency (RF) magnetron sputtering. This sputtering process was carried out at a power of 150 W with an Ar flow of 100 sccm, and a deposition time of 1 min. After deposition, the CNT-Al_2O_3-Ag-TiO_2 composite electrode was annealed in a furnace at 350 ℃ for 30 minutes under an argon atmosphere with a flow rate of 200 sccm.

2.2. Sample Characterizations

The morphology and microstructure of the CNT-based composite materials were analyzed using scanning electron microscopy (SEM; JSM-7100F, JEOL, Tokyo, Japan) and high-resolution transmission electron microscopy (HRTEM; JEM-2100, JEOL). The crystal structures of the samples were characterized by Raman spectroscopy (DXR3, Thermo Fisher Scientific, Waltham, MA, USA). The element composition of the samples were determined using energy dispersive X-ray spectroscopy (EDS, Oxford Ultim max, Oxford, UK) and X-ray photoelectron spectroscopy (XPS; Thermo Fisher Scientific etic escalab250x, Waltham, MA, USA). The C1s peak at 284.6 eV was used as the reference for calibration.

2.3. Field emission and hydrogen sensing tests

The field emission and gas sensing performance of CNT-based composite emitters were studied using an ultra-high vacuum system equipped with molecular pumps and ion pumps. Prior to each test, the system was heated to 300 ℃ and maintained at this temperature for 12 hours to acquire a base pressure below 3×10^{-7} Pa. Both the field emission and low-pressure hydrogen sensing performance of three samples were investigated in this high-vacuum turbine system. The field emission area was set to 0.16 cm^2, and the distance between the cathode and the stainless steel anode was fixed at 300 μm. The FE current and voltage were controlled by a Keithley 244 multimeter and a Keithley 248 high-voltage power supply.

The turn-on field (E_{to}) and threshold field (E_{thr}) were defined as the electric fields required to generate emission current densities of 10 μA/cm^2 and 10 mA/cm^2, respectively. As described in our previous reports [16], hydrogen sensing tests were conducted on the three samples. First, a high current of 400 μA was applied to the sample for 5 minutes to desorb the gas from the sample surface. Subsequently, high-purity hydrogen gas (99.999%) was introduced into the vacuum chamber while maintaining the system pressure within the range of 10^{-7} Pa to 10^{-3} Pa. A low FE current at the microampere level was then applied, and the current changes were recorded. This process allowed the sensing emitter to respond to specific hydrogen partial pressures. To ensure reliable pressure sensing data, the normalized current I_N (calculated as the average value of the current obtained at the end of every 10-second interval during a specific emission cycle), was used to evaluate the hydrogen sensing performance of CNT-based samples.

3. Results and discussions

3.1. Morphologic and Structural Characterizations of CNTs and CNT-Based Nanocomposites

The SEM, Raman and EDS results of the three types of CNT-based nanocomposites were presented in Figure 1. As shown in Figure 1a, the diameter of the CNT-Al_2O_3 sample ranged from 20 to 30 nm, and the carbon nanotubes were entangled with each other, which could be due to the carboxylic acid treatment [16,23]. Compared to the CNT-Al_2O_3 sample, the morphologies of CNT-Al_2O_3-Ag and CNT-Al_2O_3-Ag-TiO_2 samples did not exhibit significant differences (Figures 1b and 1c). Figure 1d exhibited the cross-section of the CNT-Al_2O_3-Ag-TiO_2 composite, demonstrating strong adhesion between the CNT-

Al_2O_3-Ag-TiO_2 layer and the silicon substrate. In Figure 1e, the Raman spectra of the three samples displayed CNT characteristic peaks, specifically the D band (1345 cm^{-1}) and G band (1582 cm^{-1}). The D band corresponds to the defects in the carbon lattice, while the G band represents the in-plane stretching vibration of sp^2 hybridized carbon atoms [23,24]. The intensity ratio of the D band to the G band (I_D/I_G) is an indicator of defect density in CNTs, a higher I_D/I_G ratio indicates more defects. The I_D/I_G ratios of the three CNT-based composite materials were nearly identical, suggesting that the crystal structure of the CNTs remained largely unchanged during the fabrication process. The EDS characterizations of all samples were shown in Figure 1f. For the CNT-Al_2O_3 sample, EDS detected the signals for C, O, Al and Si. The Si and Al signals originated from the silicon substrate and Al_2O_3, respectively, while the O signal was attributed to the Al_2O_3, and the surface contamination of carbon nanotubes resulting from the carboxylic acid treatment and exposure to air. In the CNT-Al_2O_3-Ag sample, the additional Ag signals were observed. For the CNT-Al_2O_3-Ag-TiO_2 sample, Ti signal were also detected, confirming the presence of Ti element.

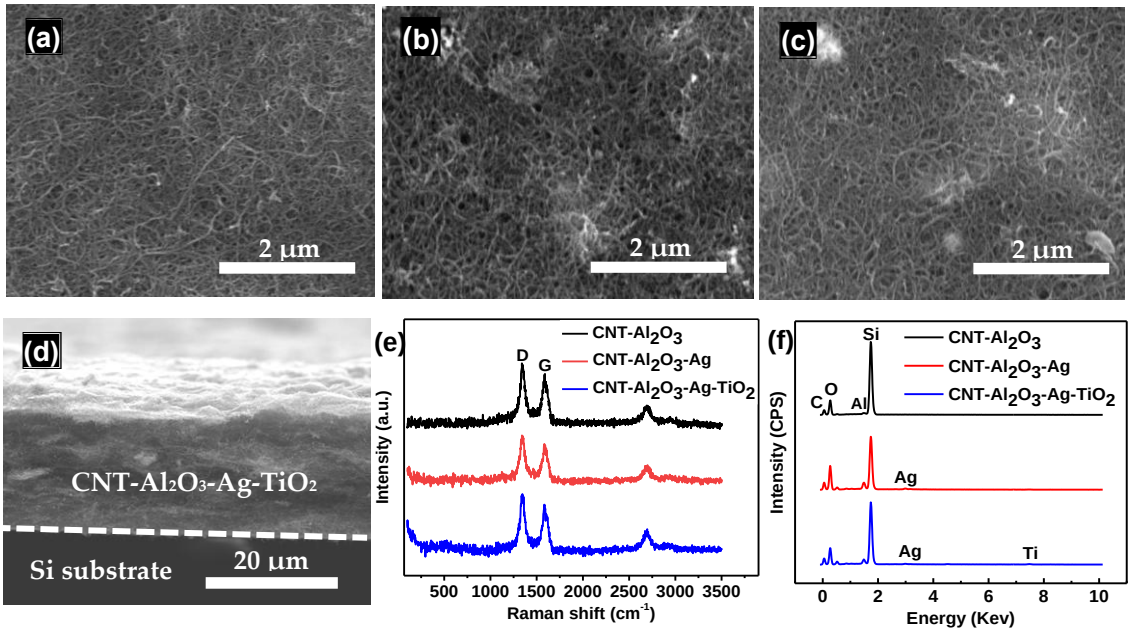

Figure 1. SEM, Raman and EDS characterizations of the CNT-Al_2O_3, CNT-Al_2O_3-Ag and CNT-Al_2O_3-Ag-TiO_2 composites. SEM images of (**a**) the CNT-Al_2O_3 composite; (**b**) the CNT-Al_2O_3-Ag composite; and (**c**) the CNT-Al_2O_3-Ag-TiO_2 composite; (**d**) Cross-sectional SEM image of the CNT-Al_2O_3-Ag-TiO_2 composite; (**e**) Raman spectra and (f) EDS spectra of the CNT-Al_2O_3, CNT-Al_2O_3-Ag and CNT-Al_2O_3-Ag-TiO_2 composites.

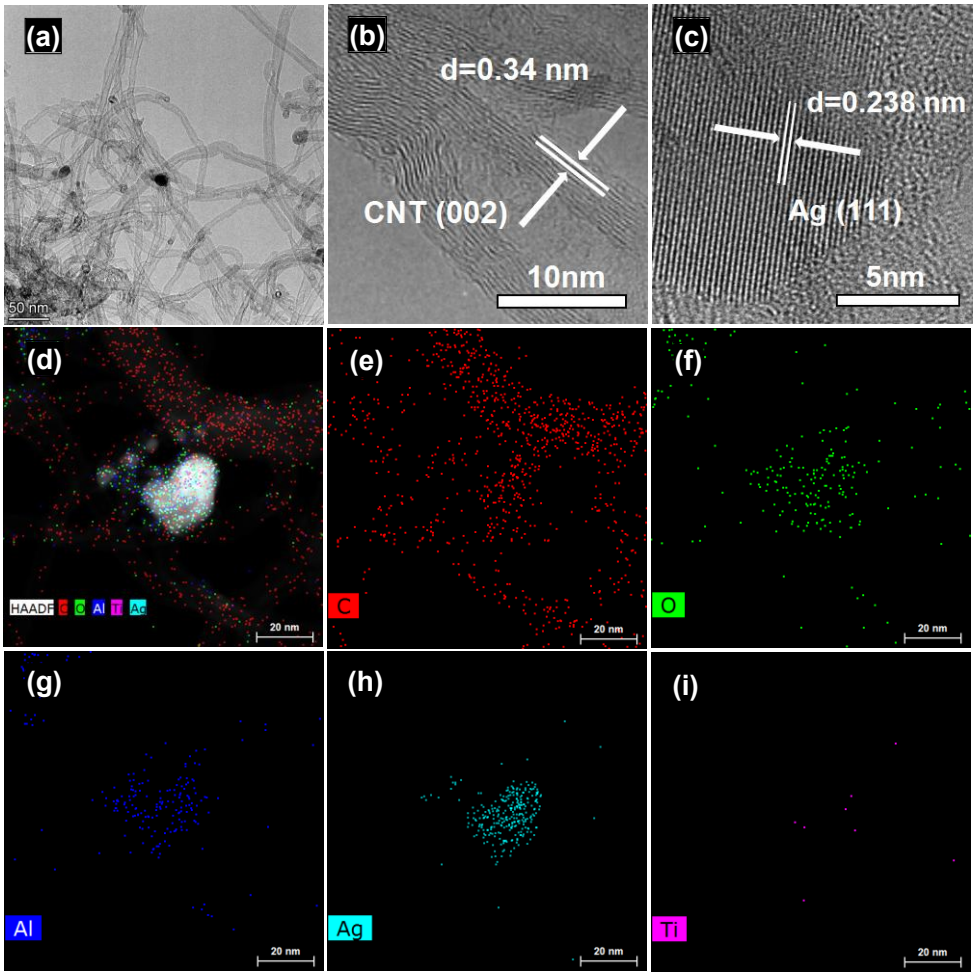

Figure 2. TEM images and EDS mapping analysis of the CNT-Al_2O_3-Ag-TiO_2 composite. (**a**) Low-resolution TEM image of the CNT-Al_2O_3-Ag-TiO_2 sample; (**b**) HRTEM image of the CNTs; (**c**) HRTEM image of the Ag nanoparticle; (**d–i**) EDS element mappings of C, O, Al, Ag and Ti elements in the CNT-Al_2O_3-Ag-TiO_2 composite.

TEM and EDS mapping of CNT-Al_2O_3-Ag-TiO_2 nanocomposites were presented in Figure 2. The diameter of CNTs was observed to be about 20-30 nm. The carbon nanotubes grew along the [002] direction, exhibiting a lattice spacing of about 0.34 nm. The HRTEM image of CNT-Al_2O_3-Ag-TiO_2 sample revealed that Ag nanoparticles, with a diameter of around 4 nm, adhered to the CNT surface. These nanoparticles displayed a lattice spacing of approximately 0.238 nm, corresponding to the (111) plane of Ag (Figure 2c) [16]. The composition of CNT-Al_2O_3-Ag-TiO_2 samples was further characterized using EDS mapping (Figures 3d-i), which confirmed the presence of the expected elements: C, O, Al, Ag, and Ti.

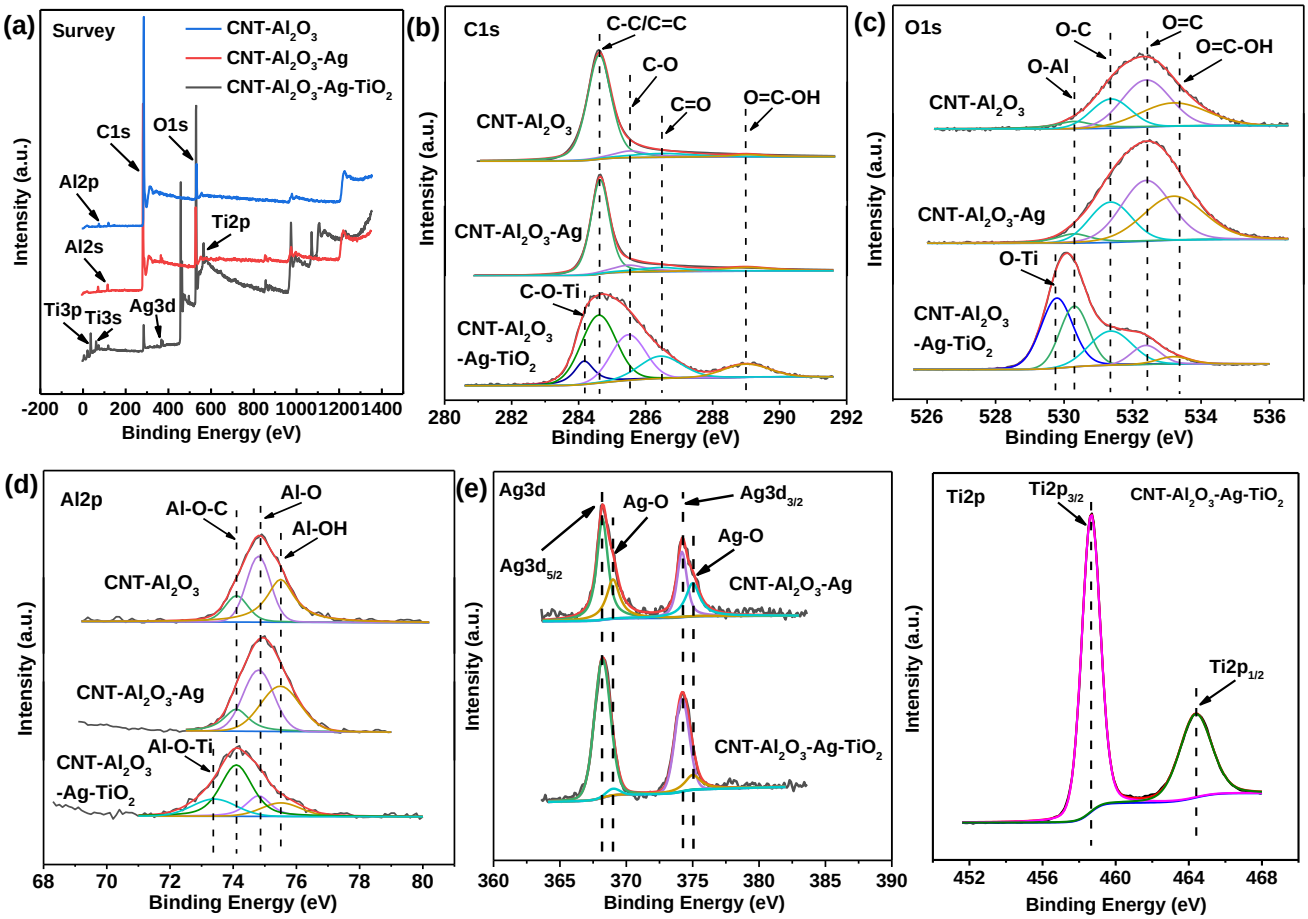

Figure 3. XPS spectra of the CNT-Al_2O_3, CNT-Al_2O_3-Ag and CNT-Al_2O_3-Ag-TiO_2 samples. (**a**) Survey; (**b**) C1s; (**c**) O1s; (**d**) Al2p; (**e**) Ag3d and (**f**) Ti2p.

Further analysis of CNT-Al_2O_3, CNT-Al_2O_3-Ag, and CNT-Al_2O_3-Ag-TiO_2 nanocomposites was conducted using XPS characterization, as shown in Figure 3. In Figure 3a, the detected signal corresponded to the expected elements: C, O, Al, Ag, and Ti. For the C1s spectra (Figure 3b), the dominant peak at 284.6 eV was attributed to the C-C/C=C bonds, while three minor peaks at 285.8, 286.4 and 289.0 eV were assigned to C-O, C=O and O=C-OH [23,25,26], respectively, for the CNT-Al_2O_3 and CNT-Al_2O_3-Ag samples. In the CNT-Al_2O_3-Ag-TiO_2 sample, an additional peak at 284.2 eV was observed, corresponding to the C-O-Ti bonds [27-29]. For the O1s spectra (Figure 3c), four peaks at 530.3, 531.4, 532.4 and 533.2 eV were attributed to the O-Al, O-C, O=C and O=C-OH bonds [26,30,31], respectively, in the CNT-Al_2O_3 and CNT-Al_2O_3-Ag samples. In the CNT-Al_2O_3-Ag-TiO_2 sample, an additional peak at 529.8 eV was identified, corresponding to the O-Ti bonds [28,29]. For the Al2p spectra (Figure 3d), three peaks at 74.1, 74.8 and 75.5 eV were assigned to the Al-O-C, Al-O and Al-OH bonds [30-32], respectively, in the CNT-Al_2O_3 and CNT-Al_2O_3-Ag samples. In the CNT-Al_2O_3-Ag-TiO_2 sample, an additional peak at 73.4 eV was observed, attributed to Al-O-Ti bonds. For the Ag3d spectra (Figure 3e), the binding energies (BE) at 374.4 eV and 364.4 eV corresponded to $Ag3d_{3/2}$ and $Ag3d_{5/2}$, indicating the presence of metallic silver [16]. For the Ti2p spectra (Figure 3f), the two peaks located at 464.4 and 458.6 eV were assigned to $Ti2p_{1/2}$ and $Ti2p_{3/2}$ [29], respectively, confirming the presence of TiO_2 in the CNT-Al_2O_3-Ag-TiO_2 composite.

3.2. Field Emission Performance Test

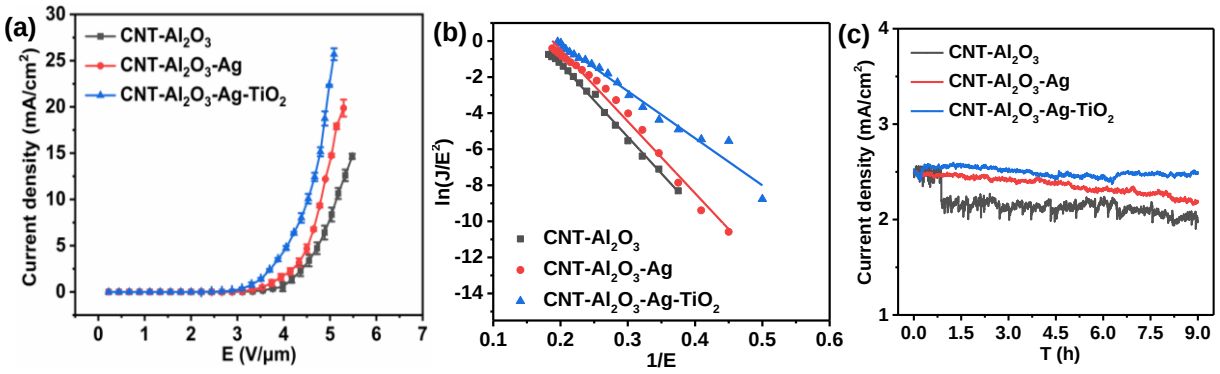

Figure 4. Field emission performances of the CNT-Al_2O_3, CNT-Al_2O_3-Ag and CNT-Al_2O_3-Ag-TiO_2 samples. (**a**) Current densities versus electric field (J-E) curves; (**b**) Fowler-Nordheim (F-N) plots; and (**c**) field emission stability under an oxygen environment at a pressure of 2×10^{-6} Pa.

Table 1. Comparison of FE parameters of CNT−based composites

Sample	Turn-on Field (V/μm)	Threshold Field (V/μm)	β
CNT-Al_2O_3	3.11	5.19	1706
CNT-Al_2O_3-Ag	2.66	4.90	1699
CNT-Al_2O_3-Ag-TiO_2	2.10	4.76	2290

Table 2. Comparison of FE parameters of other CNT−based composites

Sample	Turn-on Field (V/μm)	Threshold Field (V/μm)	β	Ref.
CNT-Pd	2.7	5.3	1900	34
CNT-ZnO	3.72	/	2082	35
α-Fe_2O_3 /CNTs*	1.211	3.23	8658	36
CNT−Graphene#	2.9	3.3	1373	37
CNT-MgO-Ag-BaO	3.32	5.92	1417	16
CNT-Al_2O_3-Ag-TiO_2	2.10	4.76	2290	this paper

Note: *E_{thr} was defined as the electric fields required to generate emission current densities of 1 mA/cm^2; #E_{thr} was defined as the electric fields required to generate emission current densities of 0.1 mA/cm^2.

The FE performances, including current density versus applied field (J-E), Fowler Nordheim (F-N) curves, and FE stability, were studied, as shown in Figure 4. The turn-on field (E_{to}) is defined as the electric fields required to achieve an emission current density of 10 μA.cm^{-2}, while the threshold field (E_{thr}) is defined as the electric fields needed to get an emission current density of 10 mA.cm^{-2}. To ensure the measurement reproducibility, the FE properties of the CNT-based samples were measured three times, and the averaged

results were presented for comparison (Table 1).The J-E curves in Figure S1 (Supplementary Material SM-1) confirm good FE repeatabilities for all three samples, showing minor variations in J-E curves after three test cycles (see error bars in Figure 4a). Compared to other CNT-based samples, the CNT-Al_2O_3-Ag-TiO_2 composite exhibited best FE performance, with a minimum E_{to} and E_{th} of 2.10 and 4.76 V/μm, respectively (Figure 4a, see Table 1). Compared to CNT-Al_2O_3-Ag (21.22-6.60=4.62eV, Figures 5b,d), the CNT-Al_2O_3-Ag-TiO_2 composite exhibited lower work function (21.22–16.97=4.25 eV, Figures 5c,f) and more emission sites due to the TiO_2 incorporation, similar to the enhanced FE properties for CNT-TiO_2 [33]. Furthermore, compared to the CNT-Al_2O_3 sample, the CNT-Al_2O_3-Ag cathode has more emission sites and the lower surface resistance due to the introduction of Ag, similar cases could be observed in the CNT-MgO-Ag composite [16] , leading to better FE properties. Compared with the FE performances of other CNT-based nanomaterials [16, 34-37], the CNT-Al_2O_3-Ag emitters in our experiment exhibited a lower turn on fields (See Table 2). Further efforts should be focuses on the further improvement of the turn on fields to match the excellent turn-on field of other one-dimensional nanomaterials [36].

As shown in Fig. 4b, the Fowler Nordheim (F-N) curves of all cathodes exhibit a linear relationship, indicating that all CNT based emitters follow the ideal FE process. The field enhancement factor (β) is considered a key parameter for evacuating the cathode materials and can be calculated using the F-N formula [16,26]:

$$\beta=-6.83\times10^{3}\times\phi^{3/2}/\text{slope} \quad (1)$$

where β is the field enhancement factor, ϕ is the work function of the cathode material, and the slope is obtained from the F-N curves. The work functions of CNT-Al_2O_3, CNT-Al_2O_3-Ag, and CNT-Al_2O_3-Ag-TiO_2 composites were estimated to be about 4.68, 4.62 and 4.25 eV, respectively (Figure 5). Based on the F-N formula, the estimated β values for the CNT-Al_2O_3, CNT-Al_2O_3-Ag, and CNT-Al_2O_3-Ag-TiO_2 samples are approximately 1706, 1699, and 2290, respectively.

The investigation of emission stability under oxygen environments is important for practical field emission applications, as the oxygen exposure represents a key challenge for device reliability.The emission stability of all CNT based field emitters was studied under an oxygen pressure of 8×10^{-6} Pa, as shown in Figure 4c. For the CNT-Al_2O_3 sample, the current decreased by 17.6% after 8 hours of emission. The current decay is possibly due to a combination of oxygen etching and local thermal effects. Compared to the CNT-Al_2O_3 sample, the CNT-Al_2O_3-Ag sample showed lower current fluctuations (8.5%), benefiting from its good thermal conductivity from Ag [16]. Because the high thermal conductivity of this sample could transfer the Joule heat during the FE process more efficiently to reduce the damage of the CNT-based sample [16]. The CNT-Al_2O_3-Ag-TiO_2 sample exhibited best stability with current fluctuations about 2% at a current density of 2.5 mA/cm², which was probably due to the enhanced oxidation resistance [20]. These experimental results suggest the CNT-Al_2O_3-Ag-TiO_2 cathod material could serve as a reliable field emission source in oxygen-containing vacuum conditions.

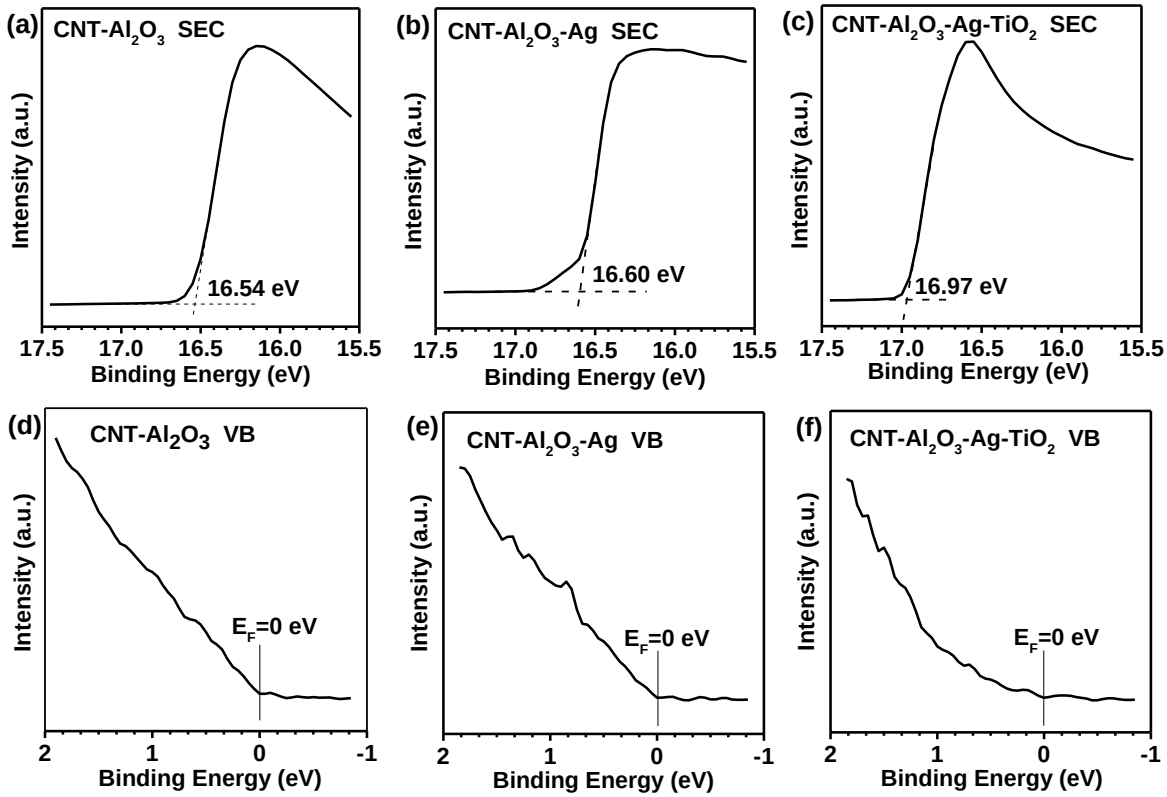

Figure 5. UPS measurements of the (**a,d**) CNT-Al_2O_3, (**b,e**) CNT-Al_2O_3-Ag and (**c,f**) CNT-Al_2O_3-Ag-TiO_2 samples. Note: SEC, VB and E_F refer to the secondary electron cutoff, valence band and Fermi level, respectively.

To determine the work function values, UPS measurements were conducted for the CNT-Al_2O_3, CNT-Al_2O_3-Ag, and CNT-Al_2O_3-Ag-TiO_2 composites, as shown in Fig.5. To obtain the secondary electron cutoff (SEC), a bias of −5 V were applied to these samples. Additionally, the Fermi levels (E_F) of all samples were calibrated to 0 eV. The work functions were then calculated using the following equation [16,38]:

$$\phi = 21.22 - BE_{SEC} \quad (1)$$

where ϕ is the work function off the material, and BE_{SEC} is the binding energy of SEC. Taking the CNT-Al_2O_3 sample as an example (Figures 5a and 5d), the work function was calculated as 4.68 eV (21.22−16.54=4.68 eV). Similarly, the work functions for CNT-Al_2O_3-Ag, and CNT-Al_2O_3-Ag-TiO_2 composites were determined to be 4.62 and 4.25 eV, respectively.

3.3. Hydrogen Sensing Performance Test

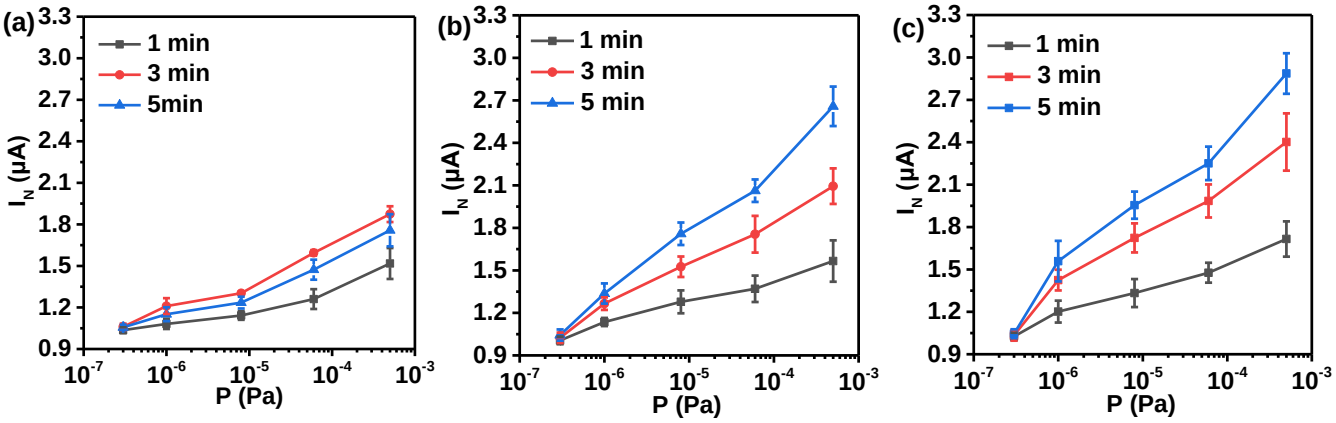

Figure 6. Pressure sensing performances for all samples. (**a**) CNT-Al_2O_3; (**b**) CNT-Al_2O_3-Ag; and (**c**) CNT-Al_2O_3-Ag-TiO_2.

Table 3. Comparison of hydrogen sensing performances of CNT-based samples under the pressure of 5.0×10^{-4} Pa

Sample	1min	3min	5min	Ref.
CNT-Al_2O_3	47%	60%	76%	This paper
CNT-Al_2O_3-Ag	58%	103%	156%	This paper
CNT-Al_2O_3-Ag-TiO_2	68%	133%	176%	This paper
CNT-MgO-Ag-BaO	67%	120%	164%	16

All samples were tested for hydrogen sensing between 10^{-7} and 10^{-4} Pa at an initial emission current of 1.0 μA (Figure 6). To ensure reliable sensing at low emission currents, the normalized average current (I_N) was utilized [8,16] and the sensing curves of all composites with six groups of test on the same sample, showing minor deviations for these samples (see Figures S3, S4 and S5 in supplementary material). Furthermore, to demonstrate the superior sensing performance of the CNT-Al_2O_3-Ag-TiO_2 composite compared to other CNT-based samples, error bars were added in the sensing curves. It could be noticed that the shapes of the pressure sensing curves were different for three CNT-based samples, which could be attributed to two primary factors. Firstly, the low-pressure hydrogen sensing occurs through gas adsorption-induced work function changes, thereby increasing emission current and producing the sensing response. Consequently, the characteristics of cathodic materials significantly influence the shape of sensing curves. Secondly, the normalized sensing current (I_N) represents an averaged value of measurements during the sensing test, rather than direct sensing current. Thus, the sensing curves with different shapes may appear. As illustrated in Figure 6, the sensing currents of all samples increased with rising hydrogen pressure from 10^{-7}-10^{-4} Pa, indicating that all samples exhibit hydrogen sensing capabilities (Table 3). As shown in Figure 6a, the CNT-Al_2O_3 sample showed the I_N increases of 47%, 60%, and 76% for 1, 3, and 5 min emissions under the pressure of 5.0×10^{-4} Pa, respectively, while the CNT-Al_2O_3-Ag samples exhibited the I_N increase of 58%, 103% and 156%, respectively, under the same conditions. This enhancement could be attributed to the better catalytic activity of Ag [16,39]. Because silver could facilitate the dissociation of hydrogen molecules into atomic hydrogen during the FE process. The adsorption of these hydrogen atoms on CNT-based nanomaterials reduces their effective work function, resulting in enhanced field emission current (sensing current). Furthermore, at the same pressure conditions, the CNT-Al_2O_3-Ag-TiO_2 sample demonstrated the best sensing performance, with the I_N increase of 68%, 133% and 176% for 1, 3, and 5 min emissions, respectively, probably due to the introduction of additional TiO_2 active sites [40]. When TiO_2 nanoparticles were introduced, they adsorbed the hydrogen atoms produced by both Joule heating and silver catalytic effects, leading to further work function decrease of the CNT-Al_2O_3-Ag composite. In comparison with the CNT-MgO-Ag-BaO composite, the sensing current of the CNT-Al_2O_3-Ag-TiO_2 sample showed higher current-increase amplitude under the same conditions (Table 3). Additionally, the CNT-Al_2O_3-Ag-TiO_2 sample achieved an 87% increase in sensing current at a pressure 8×10^{-6} Pa within 5 min, suggesting its high sensitivity for low pressure hydrogen detection. Therefore, the CNT-Al_2O_3-Ag-TiO_2 composite FE cathodes provide a promising approach to develop practical FE cathodes with low-power consumption and good low-pressure hydrogen sensing effect.

4. Conclusions

The CNT-Al_2O_3-Ag-TiO_2 composite nanomaterial developed in this study demonstrated good field emission properties and excellent low pressure hydrogen detection capabilities. This composite exhibited the best field emission characteristics with a low turn-on field of 2.1 V/μm and a threshold field of 4.76 V/μm. Furthermore, the CNT-Al_2O_3-Ag-

TiO_2 composite exhibited good emission stability with current fluctuations of about 2% under the current density of 2.5 mA/cm² and oxygen pressure of 8×10^{-6} Pa. In the hydrogen pressure detection experiments, this composite demonstrated high sensing performance with current enhancements of 176% and 87% within 5-minutess at hydrogen pressures of 5×10^{-4} Pa and 8×10^{-6} Pa, respectively. These results demonstrated application potentials of the material in two different fields, that is, robust field emitters for harsh vacuum environments and high sensitive hydrogen sensors capable of low pressure detection.

Supplementary Materials: The following supporting information can be downloaded at: www.mdpi.com/xxx/s1, Figure S1: The FE repeatability for all three samples. Figure S2: The variation curves between the sensing current and the time under different partial pressure of hydrogen for CNT-Al_2O_3-Ag-TiO_2. Figure S3: Pressure sensing performances for CNT-Al_2O_3 with six groups of test on the same sample with different test time. Figure S4: Pressure sensing performances for CNT-Al_2O_3-Ag with six groups of test on the same sample with different test time. Figure S5: Pressure sensing performances for CNT-Al_2O_3-Ag-TiO_2 with six groups of test on the same sample with different test time.

Author Contributions: Conceptualization, C.D. and W.Q.; software, Y.W..; investigation, Y.W., Z.T., Y.J., and W.H.; writing—original draft preparation, Y.W. and W.Q.; writing—review and editing, C.D.; visualization, C.D., W.Q., and Y.W.; supervision, C.D. and W.Q.; project administration, C.D. and W.Q.; funding acquisition, C.D. and W.Q. All authors have read and agreed to the published version of the manuscript.

Funding: This research was funded by the National Natural Science Foundation of China (Grant No. 61871292, 62374118).

Institutional Review Board Statement: Not applicable.

Informed Consent Statement: Not applicable.

Data Availability Statement: The original contributions presented in the study are included in the article, further inquiries can be directed to the corresponding author.

Conflicts of Interest: The authors declare no conflicts of interest.

References

1. Thapa, A.; Poudel, Y. R.; Guo, R.; Jungjohann, K. L.; Wang, X. W.; Li, W. Z. Direct synthesis of micropillars of vertically aligned carbon nanotubes on stainless-steel and their excellent field emission properties. *Carbon* **2021**, *171*, 188–200.
2. Girma, H. G.; Park, K. H.; Ji, D. S.; Kim, Y.; Lee, H. M.; Jeon, S.; Jung, S. H.; Kim, J. Y.; Noh, Y. Y.; Lim, B. Room-Temperature Hydrogen Sensor with High Sensitivity and Selectivity using Chemically Immobilized Monolayer Single-Walled Carbon Nanotubes. *Adv. Funct. Mater.* **2023**, *33*.
3. Dwivedi, N.; Dhand, C.; Carey, J. D.; Anderson, E. C.; Kumar, R.; Srivastava, A. K.; Malik, H. K.; Saifullah, M. S. M.; Kumar, S.; Lakshminarayanan, R.; Ramakrishna, S.; Bhatia, CS.; Danner, A. The rise of carbon materials for field emission. *J. Mater. Chem. C* **2021**, *9*, 2620–2659.
4. Bonard, J. M.; Klinke, C.; Dean, K. A.; Coll, B. F. Degradation and failure of carbon nanotube field emitters. *Phys. Rev. B* **2003**, *67*, 181–183.
5. Zhang, Z.; Zhang, H.; Zhang, G.; Hou, S.; Gu, Z.; Zhao, X.; Liu, W.; Xue, Z. Influence of Oxygen on Field Emission from Single-Walled Carbon Nanotubes. *Jpn. J. Appl. Phys.* **2002**, *41*, 5755–5756.
6. Jung, D.; Han, M.; Lee, G. S. Fast-Response Room Temperature Hydrogen Gas Sensors Using Platinum-Coated Spin-Capable Carbon Nanotubes. *ACS Appl. Mater. Interfaces* **2015**, *7*, 3050–3057.
7. Zhang, Z. F.; Yang, Y. X.; Zhu, S. L.; Shi, Y.; Song, J. F.; Ren, G. K.; Deng, S. J.; Tian, X. F.; Zheng, Z. Factors that influence the performance of hydrogen detectors based on single-wall carbon nanotubes. *New Carbon Mater.* **2023**, *38*.
8. Zhao, Y.; Cai, J.; Luo, H.; Kang, S.; Qian, W.; Dong, C. Low pressure hydrogen sensing based on carbon nanotube field emission: Mechanism of atomic adsorption induced work function effects. *Carbon* **2017**, *124*, 669-674.
9. Feng, T.; Cheng, Y.; Chen, L.; Xi, Z.; Zhu, J.; Li, Y. Hydrogen adsorption characteristics of $Zr_{57}V_{36}Fe_7$ non-evaporable getters at low operating temperatures, *Vacuum* **2018**, *154*, 6-10
10. Mo, C. B.; Hwang, J. W.; Cha, S. I.; Hong, S. H. Multi-walled carbon nanotube/Co composite field emitters fabricated by in situ

spray coating. *Carbon* **2009**, *47*, 1276–1281.
11. Raza, M. M. H.; Sadiq, M.; Khan, S.; Sarvar, M.; Parveen, S.; Masheerul Aalam, S.; Zulfequar, M.; Husain, S.; Ali, J. Surface modification via silver nanoparticles attachment: An ex-situ approach for enhancing the electron field emission properties of CNT field emitters. *Mater. Today Proc*. **2021**, *47*, 1542–1549.
12. Gurylev, V.; Chin, T. K.; Tsai, H. Y. Carbon Nanotubes Decorated with Platinum Nanoparticles for Field-Emission Application. *ACS Omega* **2019**, *4*, 15428–15434.
13. Wu, Y. S.; Jun, L.; Ye, J. C.; Song, Y. J.; Chen, X. H.; Huang, S. M.; Zhuo, S.; Wei, O. Y. Outstanding field emission properties of titanium dioxide /carbon nanotube composite cathodes on 3D nickel foam. *J. Alloy. Compd.* **2017**, *726*, 675–679.
14. Jiang, J. L.; Fang, H. Q.; Zhang, X.; He, K. C.; Wei, Z. Q.; Pang, X. J.; Dai, J. F. Electrochemical synthesis of aligned amorphous carbon nanotubes/TiO_2 nanotubes heterostructured arrays and its field emission properties. *Diam. Relat. Mater.* **2017**, *74*, 205–211.
15. Gurylev, V.; Chin, T. K.; Useinov, A. Charge transfer and field emission characteristics of TiO_2@CNTs nanocomposite: Effect of TiO_2 crystallinity. *J. Alloys Compd*. **2021**, *857*.
16. Liu, X.; Qian, W.; Chen, Y.; Dong, M.; Yu, T.; Huang, W.; Dong, C. Construction of CNT-MgO-Ag-BaO Nanocomposite with Enhanced Field Emission and Hydrogen Sensing Performances. *Nanomaterials* **2023**, *13*.
17. Song, G.; Xu, G. Q.; Quan, Y. K.; Yuan, Q. C.; Davies, P. A. Uniform design for the optimization of Al_2O_3 nanofilms produced by electrophoretic deposition. *Surf. Coat. Tech.* **2016**, *286*, 268–278.
18. Cui, H.; Gong, L.; Yang, G.; Sun, Y.; Chen, J. and Wang, C. Enhanced field emission property of a novel Al_2O_3 nanoparticle-decorated tubular SiC emitter with low turn-on and threshold field. *Phys. Chem. Chem. Phys.* **2011**, *13*, 985-990.
19. Rahman, R.; Aslam, J.; Khokhar, M.; et al. Synthesis and simulation study of titanium dioxide-based nanomaterial for electron carrier selective contact solar cell. *Inorg.Chem. Commun.* **2024**, *169*, 112863.
20. Nguyen, Q. X.; Nguyen, T. T.; Pham, N. M.; Khong, T. T.; Cao, T. M.; Van Pham, V. A fabrication of CNTs/TiO_2/polyurethane films toward antibacterial and protective coatings. *Prog. Org. Coat*. **2022**, *167*.
21. Cao, F.; Zhang, H. Y.; Duan, X.; Li, X. K.; Ding, R.; Hua, K.; Rui, Z. Y.; Wu, Y. K.; Yuan, M. C.; Wang, J. K.; et al. Coating Porous TiO_2 Films on Carbon Nanotubes to Enhance the Durability of Ultrafine PtCo/CNT Nanocatalysts for the Oxygen Reduction Reaction. *ACS Appl. Mater. Interfaces* **2022**, *14*, 51975–51982.
22. Haidry, A.; Xie, L.; Wang, Z; Li, Z. Hydrogen sensing and adsorption kinetics on ordered mesoporous anatase TiO_2 surface. *Appl. Surf. Sci.* **2020**, *500*, 144219.
23. Dong, M. L.; Qian, W. J.; Liu, X. Z.; Chen, Y. W.; Huang, W. J.; Dong, C. K. Enhanced thermo cell properties from N-doped carbon nanotube-Pd composite electrode. *Surf. Coat. Tech.* **2022**, *434*.
24. Zhao, F.; Qian, W. J.; Li, M. J.; Li, W.; Chen, L. H.; Zhong, F. Y.; Huang, W. J.; Dong, C. K. Directly grown carbon nanotube based hybrid electrodes with enhanced thermo-cell performances. *RSC. Adv.* **2017**, *7*, 23890–23895.
25. Qian, W. J.; Li, M. J.; Chen, L. H.; Zhang, J. H.; Dong, C. K. Improving thermo-electrochemical cell performance by constructing Ag-MgO-CNTs nanocomposite electrodes. *RSC. Adv*. **2015**, *5*, 97982–97987.
26. Huang, W. J.; Qian, W. J.; Luo, H. J.; Dong, M. L.; Shao, H. Z.; Chen, Y. W.; Liu, X. Z.; Dong, C. K. Field emission enhancement from directly grown N-doped carbon nanotubes on stainless steel substrates. *Vacuum* **2022**, 198.
27. Yang, H. P.; Wu, S.; Duan, Y. P.; Fu, X. F.; Wu, J. M. Surface modification of CNTs and enhanced photocatalytic activity of TiO_2 coated on hydrophilically modified CNTs. *Appl. Surf. Sci.* **2012**, *258*, 3012–3018.
28. Liu, Y.; Elzatahry, A. A.; Luo, W.; Lan, K.; Zhang, P. F.; Fan, J. W.; Wei, Y.; Wang, C.; Deng, Y. H.; Zheng, G. F.; et al. Surfactant-templating strategy for ultrathin mesoporous TiO_2 coating on flexible graphitized carbon supports for high-performance lithium-ion battery. *Nano Energy* **2016**, *25*, 80–90.
29. Chen, J.; Wang, E. Q.; Mu, J. C.; Ai, B.; Zhang, T. Z.; Ge, W. Q. CNTs–C@TiO_2 composites with 3D networks as anode material for lithium/sodium ion batteries. *J. Mater. Sci.* **2019**, *54*, 592–604.
30. Wang, S. F.; Zhang, C. F.; Sun, G. G.; Yuan, Y. G.; Chen, L.; Xiang, X.; Ding, Q. P.; Chen, B.; Li, Z. J.; Zu, X. T. Self-assembling synthesis of α-Al_2O_3–carbon composites and a method to increase their photoluminescence. *J. Lumin.* **2014**, *153*, 393–400.
31. Lee, B.; Park, S. Y.; Kim, H. C.; Cho, K. J.; Vogel, E. M.; Kim, M. J.; Wallace, R. M.; Kim, J. Conformal Al_2O_3 dielectric layer deposited by atomic layer deposition for graphene-based nanoelectronics. *Appl. Phys. Lett.* **2008**, *92*, 208–210.
32. Zhao, Z.; Peng, D.; Zhi, Y.; Hao, X.; Wan, S.; Yue, M.; Kuang, J.; Xuan, W.; Zhu, L.; Cao, W. Synergistic effects of oriented AlN skeletons and 1D SiC nanowires for enhancing the thermal conductivity of epoxy composites. *J. Alloy. Compd.* **2023**, *963*.

33. Wu, Y.; Li, J.; Ye, J.; Song, Y.; Chen, X.; Huang, S.; Sun, Z.; Ou-Yang, W. Outstanding field emission properties of titanium dioxide /carbon nanotube composite cathodes on 3D nickel foam. *J. Alloy. Compd.* **2017**, *726*, 675-679.
34. Wong, Y. ; Wei, S.; Kang, W.; Davidson, J.; Hofmeister, W.; Huang, J.; Cui, Y. Carbon nanotubes field emission devices grown by thermal CVD with palladium as catalysts. *Diam. Relat. Mater.* **2004,** *13* (11-12), 2105-2112.
35. Huang, C.; Yeh, C.; Chang, Y.; Hsieh, Y.; Ku, C.; Lai, Q. Field emission properties of CNT-ZnO composite materials. *Diam. Relat. Mater.* **2009**, *18*, 452-456.
36. Guo, F.; Ye, Y.; Yang, Z.; Hong, C.; Hu, L.; Wu, C.; Guo, T. The in situ preparation of novel α-Fe_2O_3 nanorods/CNTs composites and their greatly enhanced field emission properties. *Appl. Surf. Sci.* **2013**, *270*, 621-626.
37. Nguyen, D.; Tai, N.; Chen, S.; Chueh, Y. Controlled growth of carbon nanotube–graphene hybrid materials for flexible and transparent conductors and electron field emitters. *Nanoscale* **2012,** *4*, 632-638.
38. Tu, Y. Q.; Qian, W. J.; Dong, M. L.; Chen, G. T.; Quan, Y. L.; Huang, W. J.; Dong, C. K. Enhanced Field Emission and Low-Pressure Hydrogen Sensing Properties from Al-N-Co-Doped ZnO Nanorods. *Nanomaterials* **2024**, *14,* 863.
39. Yang, G. W.; Gao, G. Y.; Wang, C.; Xu, C. L.; Li, H. L. Controllable deposition of Ag nanoparticles on carbon nanotubes as a catalyst for hydrazine oxidation. *Carbon* **2008**, *46*, 747–752.
40. Abdulhameed, A.; Mahnashi, Y. Fabrication of carbon nanotube/titanium dioxide nanomaterials-based hydrogen sensor using novel two-stage dielectrophoresis process. *Mat. Sci. Semicon. Proc.* **2023**, *167*, 107794.